Available online at www.sciencedirect.com
ScienceDirect
Journal of Photochemistry and Photobiology A: Chemistry 194 (2008) 200–205
Journal of Photochemistry and Photobiology A:Chemistry
www.elsevier.com/locate/jphotochem

UV laser photolysis of 1,3-butadiyne and formation of a polyoxocarbosilane-doped nanosized carbon

Josef Pola [a,*], Anna Galíková [a], Zdeněk Bastl [b], Vladimír Vorlíček [c], Jan Šubrt [d], Snejana Bakardjieva [d], Akihiko Ouchi [e]

[a] *Laboratory of Laser Chemistry, Institute of Chemical Process Fundamentals, Academy of Sciences of the Czech Republic, 16502 Prague, Czech Republic*
[b] *J. Heyrovský Institute of Physical Chemistry, Academy of Sciences of the Czech Republic, 18223 Prague 8, Czech Republic*
[c] *Institute of Physics, Academy of Sciences of the Czech Republic, 18223 Prague 8, Czech Republic*
[d] *Institute of Inorganic Chemistry, Academy of Sciences of the Czech Republic, 25068 Řež, Czech Republic*
[e] *National Institute of Advanced Industrial Science and Technology, AIST, Tsukuba, Ibaraki 305-8565, Japan*

Received 4 June 2007; received in revised form 6 August 2007; accepted 7 August 2007
Available online 10 August 2007

Abstract

Highly intense ArF laser radiation induced photolysis of gaseous 1,3-butadiyne results in the formation of a number of volatile, highly unsaturated hydrocarbons and efficient deposition of nanosized carbon soot. Minor etching of the reactor silica window by photolytic products allows doping of the depositing carbon soot by nanosized silica and polyoxocarbosilane. Upon heating to 700 °C, the photoproduct converts to partially graphitized carbon containing polyoxocarbosilane.

Keywords: Laser-induced photolysis; 1,3-Butadiyne; Nanostructured carbon; Polyoxocarbosilane; Nanocomposite

1. Introduction

Laser-induced chemical vapor deposition (LCVD) of carbonaceous materials involving interaction of intense laser radiation with gaseous hydrocarbons has recently become a well-established field. Both photolytic and thermolytic laser actions have been demonstrated.

In photolytic depositions, ArF laser photolysis of ethyne [1–3], ArF and XeCl laser photolysis of 3-butyn-2-one [4] and Ar^+ cw laser [5], XeCl laser [6] and ArF laser [7] photolysis of methylene iodide yielded amorphous hydrogenated carbon films in which the ratio of sp^3 and sp^2 states of C atoms and the hydrogen concentration was controlled by the gas phase chemistry and the structure of the edduct. Thus, the ArF laser photolysis of acetylene yields H-rich and graphite-like [1,2] or highly C (sp^3)-based [3] films, while Ar^+, KrF and ArF laser photolysis of CH_2I_2 gives rise to H-rich and fairly unsaturated C films [6,7].

In thermolytic depositions, pulsed CO_2 laser radiation was applied to induce infrared multiple-photon decomposition of 3-butyn-2-one and yielded graphitic hydrogenated film [8]. Various nanoforms of carbon were deposited from the flame generated in gaseous hydrocarbons by irradiation from powerful cw CO_2 lasers. Thus, the irradiation of ethane–H_2 and ethane–SiH_4 mixtures yielded polyaromatic species, polymers, amorphous carbon and spherical diamond particles [9], that of ethylene afforded graphitic carbon nanopowders having turbostratic structure [10] and that of ethene, 1,3-butadiene and propadiene resulted, depending on the reaction conditions, in the formation of aromatic, poorly organized, hydrogenated, turbostratic and concentric nanoparticles [11,12]. Shell-shaped carbon nanoparticles were synthesized by interaction of highly intense cw CO_2 laser radiation with ethyne [13], carbon clusters

* Corresponding author. Tel.: +420 2 20390308; fax: +420 2 20920661.
E-mail address: pola@icpf.cas.cz (J. Pola).

1010-6030/$ – see front matter © 2007 Elsevier B.V. All rights reserved.
doi:10.1016/j.jphotochem.2007.08.006

and soot particles [14] and different nanostructures contained in soot (amorphous carbon, carbon with graphenes and fullerene-like features) [15] were obtained by CO_2 laser-induced and SF_6-sensitized decomposition of ethyne and benzene. All these depositions are truly homogeneous gas phase processes and differ from LCVD processes in which gaseous hydrocarbons are decomposed on substrates heated by IR lasers (e.g. [16,17]).

In this paper we introduce a novel, easy and efficient laser-induced approach to nanostructured carbon by employing pulsed, highly intense UV laser radiation applied to gaseous 1,3-butadiyne. We show that the photoproduct contains low quantities of silica and polyoxocarbosilane ingredients and that it evolves into partially graphitic polyoxocarbosilane-doped nano-carbon when heated to 700 °C. The presented work thus represents an entry to nanosized polyoxocarbosilane–carbon composites, the materials thus far known only in the bulk glassy form as intermediates to silicon carbide.

2. Experimental

The ArF laser irradiation of gaseous 1,3-butadiyne (120 Torr) in helium (total pressure 760 Torr) was carried out using an LPX 210i laser operating at 193 nm with a pulses (energy of 220 mJ) focused to incident area 0.18 cm^2 (fluence 1.2 J/cm^2) and a repetition frequency of 10 Hz. The fluence used represents a critical threshold, since the formation of dark soot does not take place at fluences below this value. The 1,3-butadiyne–He samples were irradiated in a reactor (140 ml in volume) which was equipped with a sleeve with a rubber septum and a PTFE valve connecting it to a standard vacuum manifold and consisted of two orthogonally positioned Pyrex tubes, one fitted with two UV grade synthetic silica windows and the other furnished with two KBr windows (Fig. 1).

The progress of the 1,3-butadiene decomposition was monitored directly in the reactor by FTIR spectrometry (a Shimadzu FTIR IR Prestige-21 spectrometer) using diagnostic absorption bands of 1,3-butadiyne at 2020 and 845 cm^{-1}. The gaseous products were analyzed by gas chromatography–mass spectroscopy (a Shimadzu QP 5050 mass spectrometer (60 m caplillary column Neutrabond-1, programmed temperature 30–200 °C). Sampling was made by a gas-tight syringe (Dynatech Precision Sampling). The decomposition products were identified through their mass spectra using NIST library.

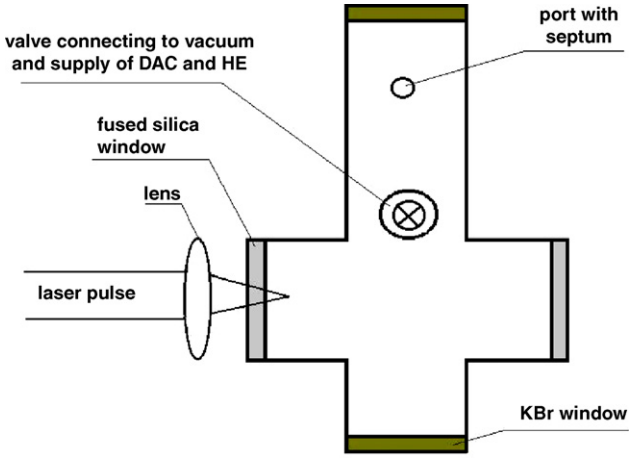

Fig. 1. Schematic of batch reactor (top view).

The deposited material was analyzed by X-ray photoelectron (XPS), Auger, FTIR and Raman spectroscopy, electron microscopy and thermogravimetry.

The X-ray C 1s, O 1s and Si 2p photoelectron and C KLL Auger electron spectra of the deposit were measured using an ESCA 310 (Scienta) electron spectrometer with a base pressure better than 10^{-7} Pa and using Al Kα radiation (1486.6 eV) for electron excitation. The surface composition of the deposited film was determined by correcting the spectral intensities for subshell photoionization cross-sections.

Raman spectra were recorded on a Renishaw (a Ramascope model 1000) Raman microscope with a CCD detector using the exciting beam of an Ar-ion laser (514.5 nm) 50 μW. The beam was attenuated to obtain incident energy densities in the range of 10^2 to 10^3 W/cm^2.

SEM analyses were carried out by using a Philips XL30 CP scanning electron microscope equipped with energy-dispersive analyzer (EDAX DX-4) of X-ray radiation. A PV 9760/77 detector in low vacuum mode (0.5 mbar) was used for quantitative determination of Si, C and O elements.

Transmission electron micrographs were obtained using a JEOL JEM 3010 microscope operating at an accelerating voltage of 300 kV.

Thermogravimetric analysis of the solid deposit (sample weight 0.5 mg) was conducted by heating the sample up to 700 °C at the rate of 4 °C/min, using Cahn D-200 recording microbalances in a stream of argon.

FTIR spectra of the deposit and the residue after TGA analysis were acquired on a Nicolet Impact FTIR spectrometer.

1,3-Butadiyne was prepared according to the earlier reported procedure [18].

3. Results and discussion

3.1. 1,3-Butadiyne photolysis

The ArF laser irradiation of gaseous 1,3-butadiyne leads to visible luminescence, depletion of 1,3-butadiyne and efficient formation of black fog (very tiny black soot) that flows in the reactor and slowly deposits to reactor surface. The silica windows remain in the course of the irradiation clean and not deposited by a polymer [19]. This allows achieve almost complete decomposition of 1,3-butadiyne (Fig. 2).

During the irradiation, a minor depletion of silica window at the side exposed to 1,3-butadiyne vapors takes place from ca. 0.2 cm^2 area through which laser pulses penetrate to the reactor. This area is a base of ca. 1 cm long visible luminescence zone. Independent high-fluence irradiations of the reactor filled with only atmospheric pressure of He do not lead to any silica removal (spallation) and we assume that the observed silica depletion is due to interaction of excited photolytic products with the silica surface, leading to silica etching. Such a process has not yet been reported in the gas phase, although similar silica etching referred

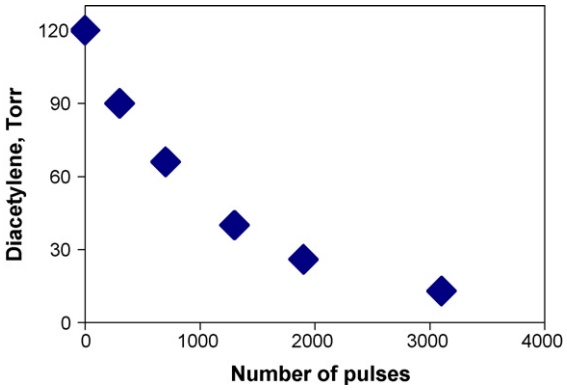

Fig. 2. Depletion of 1,3-butadiyne as dependent on number of pulses.

to as laser backside wet etching (e.g. [20–22]) was described in the liquid phase.

The volatile hydrocarbons were produced only in minor amounts (Fig. 3). This confirms that the decomposed 1,3-butadiyne is mainly consumed for the formation of the soot. The major volatile product is ethyne (less than 2% of depleted acetylene) and others, 1-buten-3-yne, 1,3-butadiyne, C_4H_4 (1,2,3-butatriene, *m/z*, intensity in (%): 52, 100; 51, 68; 50, 59; 49, 24), C_5H_4 (pentadiynes, 1,2-pentadiene-3-yne or 1,2,3,4-pentatetraene, *m/z*, intensity in (%): 64, 100; 63, 68; 62, 37; 61, 24; 38, 19), benzene, 1,3,5-hexatriyne (*m/z*, intensity in (%): 74, 100; 73, 32; 37, 27), ethynylbenzene and 1,3,5,7-octatetrayne (*m/z*, intensity in (%): 98, 100; 97, 27; 61, 29) were produced only in traces.

The assumed polyynes $H(C{\equiv}C)_nH$ and cumulenes $H_2C{=}C_n{=}CH_2$ ($n>1$) do not fairly differ in stability [23], but only the former have been proven experimentally. We thus stress that the mass spectral assignment of 1,2,3-butatriene is the first experimental support for these yet elusive molecules.

The occurrence of polyynes, cumulenes and other presumed unsaturates is in line with several possible chemistries: (i) photodimerization of C_4H_2 leading to C_8H_2 [24] ensued by photopolymerization [19], (ii) reversible isomerization of ethynes to ethylidenes [25], formation of ethynyl radicals and their recombination, H-abstraction and attack onto the π-electron density of the intermediate unsaturated (allene or acetylene bond system)

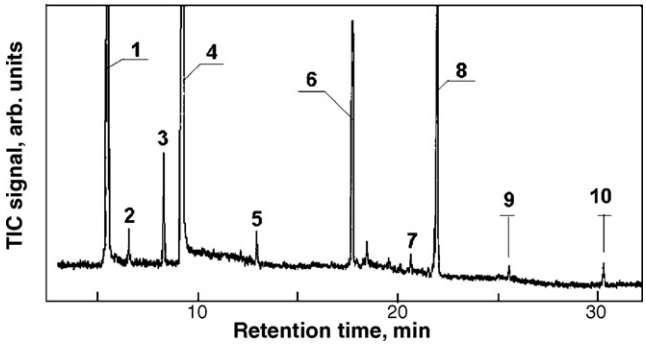

Fig. 3. GC/MS trace of volatile products (peak designation: (1) ethyne; (2) C_3H_4; (3) 1-buten-3-yne; (4) 1,3-butadiyne; (5) C_4H_4 (1,2,3-butatriene); (6) C_5H_4; (7) benzene; (8) 1,3,5-hexatriyne; (9) ethynylbenzene; (10) 1,3,5,7-octatetrayne.

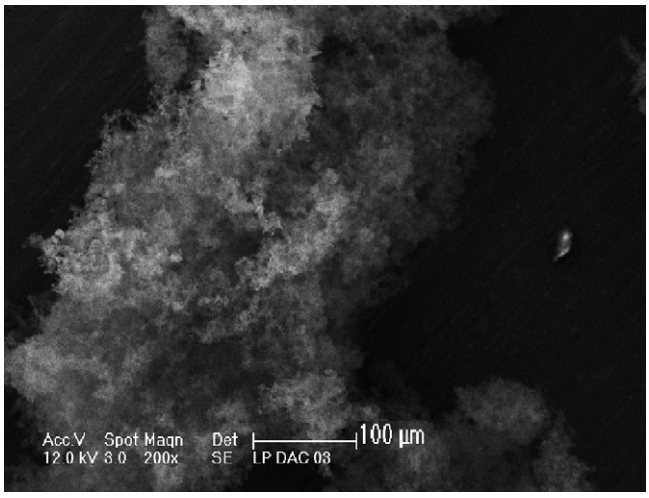

Fig. 4. SEM image of deposited soot (bar = 100 μm).

hydrocarbons [26] and (iv) photodissociation of ethynyl radical into C_2 +H [27]. The formed C_2 and highly unsaturated species are poorer in H than 1,3-butadiyne and agglomerate into the observed soot. The presence of ethynylbenzene suggests this molecule as a primary source of cyclic carbonaceous structures.

3.2. Properties of photo-deposited product

The SEM image of the soot shows fluffy spongy structure (Fig. 4). The SEM-EDX analysis is consistent with stoichiometry $C_{1.00}O_{0.07}Si_{0.02}$ and confirms the observed silica etching. The incorporation of silicon and O elements into carbon is rather low and the high BET surface area of the soot (137 m^2/g) can be therefore attributed to carbon. The TEM images and electron diffraction (Fig. 5) reveal that the fluffy structure is formed by inter-linking chains with a 10 nm diameter and that this nanostructured soot is amorphous.

The visible Raman spectra at different intensity of the exciting beam (Fig. 6) show G and D bands, respectively, centered at 1592 and 1360 cm^{-1}. The position and the broadness of the G band resemble those of graphitic a-C:H films and soot [28–30]. The latter parameter allows [31] estimate H content as ca. 5 at.%, which agrees with the substantial H loss during decomposition chemistry of buta-1,3-diyne. The G band reflects bond stretches of all pairs of sp^2 atoms in rings and chains and the D band corresponds to breathing modes of rings (e.g. [30,32]). The intensity of both bands as well as the I(D)/I(G) ratio, which is a measure of the ordering of the sp^2 phase, increase (0.58 at 100 W/cm^2, 0.67 at 250 W/cm^2, 0.65 at 500 W/cm^2 and 0.71 at 1000 W/cm^2) with increasing excitation energy density. These changes indicate that increasing temperature in the irradiated spot leads to reorganization of soot structure: more sp^2 centers are developed (or topologically ordered) and the proportion of those in rings becomes higher. Such a rise of I(D)/I(G) ratio is also consistent with a growth in number and/or size of crystallites [32] and also a loss of H. The spectrum does not show bands of high purity fused silica at 495 and 1200 cm^{-1} [33].

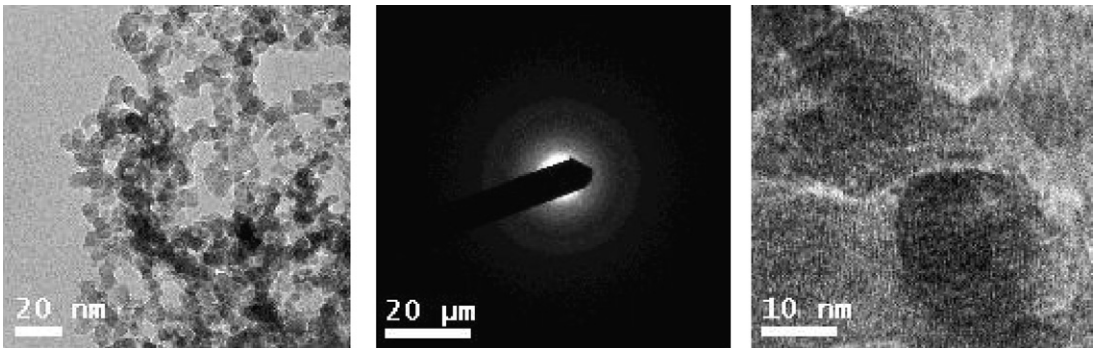

Fig. 5. TEM images and electron diffraction of deposited soot.

The XPS analysis shows that the stoichiometry in few superficial layers of the deposited soot is $C_{1.00}O_{0.21}Si_{0.03}$, which indicates a higher degree of oxidation than in the bulk soot (as derived from the EDX analysis). The Si 2p core level spectrum of the soot differs from that of silica showing peak at 103.4 eV and can be deconvoluted in two components located at 102.3 and 101.1 eV (Fig. 7). These falls into the range of values published for polyoxocarbosilanes [34,35] and are respectively assignable (e.g. [36]) to SiO_2C_2 and $SiOC_3$ structures. Using the energy difference between the most positive and most negative excursions in the C KLL derivative Auger spectra as a measure of the population of C atoms in sp^3 and sp^2 states (e.g. [37]) leads to approximately 33% of carbon atoms being present in the sp^2 states.

The IR spectrum of the soot (Fig. 8) shows sharp absorption bands peaked at 510, 600, 710, 900, 1310, 1450 and 1550 cm^{-1} together with broad bands between 1000 and 1250 cm^{-1} (splitting into contributions at 1060, 1118 and 1160 cm^{-1}), 1600–1800 cm^{-1} and 2850–3000 cm^{-1}. Although detailed assignment is difficult, the bands at 510 and 1118 cm^{-1} are respectively due to δ(OSiO) and ν^{asym}(SiOSi) modes in silica [38] and those at 1060 and 1160 cm^{-1} are respectively assignable to ν^{asym}(SiOSi) mode in siloxane-like structures [39] and to ν(C–O) modes blended with aromatic skeleton vibrations [39]. The band at 1600–1800 cm^{-1} relates to ν(C=C) and ν(C=O) modes. The ν(C–O) and ν(C=O) bands are indicative of low oxidation at the carbon and the absorption between 2850 and 3000 cm^{-1} (and none at higher wavenumbers) reveals the presence of only C(sp^3)–H bonds.

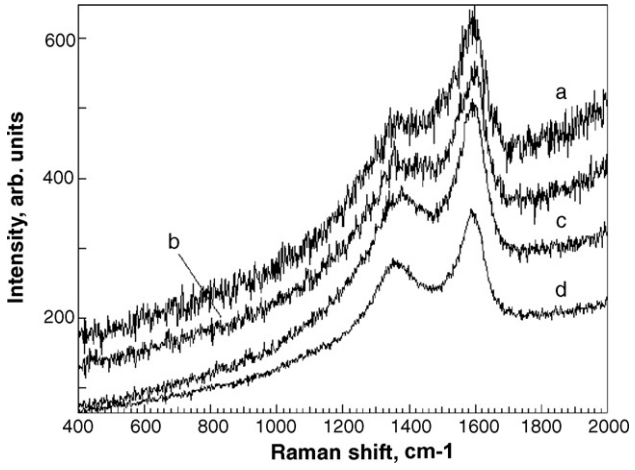

Fig. 6. Raman spectra of deposited soot at different incident energy density of exciting beam. (Intensity normalized to the same excitation energy density; (a) 100 W/cm^2; (b) 250 W/cm^2; (c) 500 W/cm^2; (d) 1000 W/cm^2).

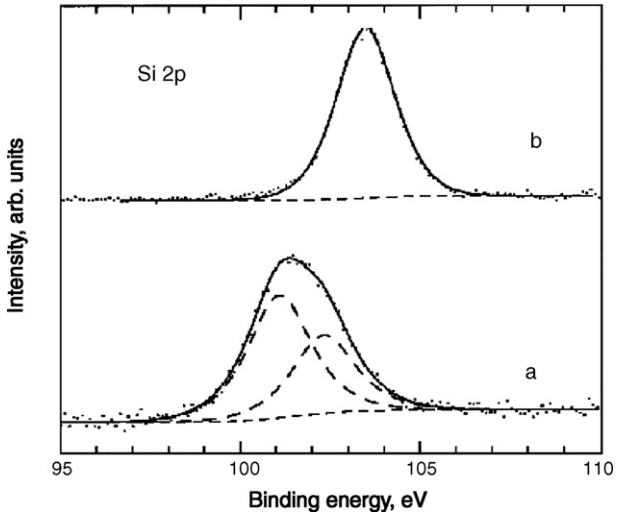

Fig. 7. Si 2p core level spectra of the deposited soot (a) and silica (b).

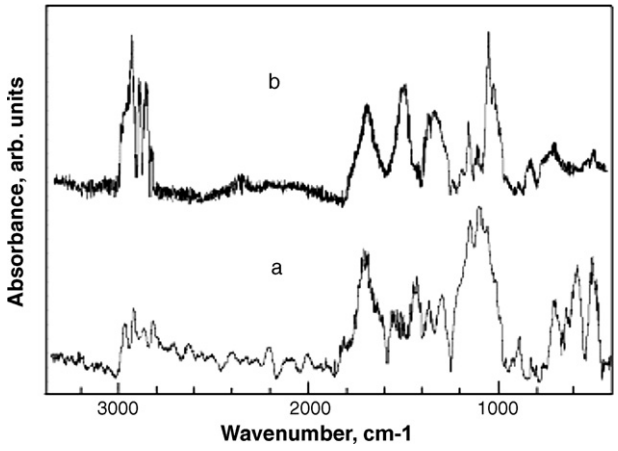

Fig. 8. FTIR spectrum of the soot before (a) and after (b) heating to 700 °C.

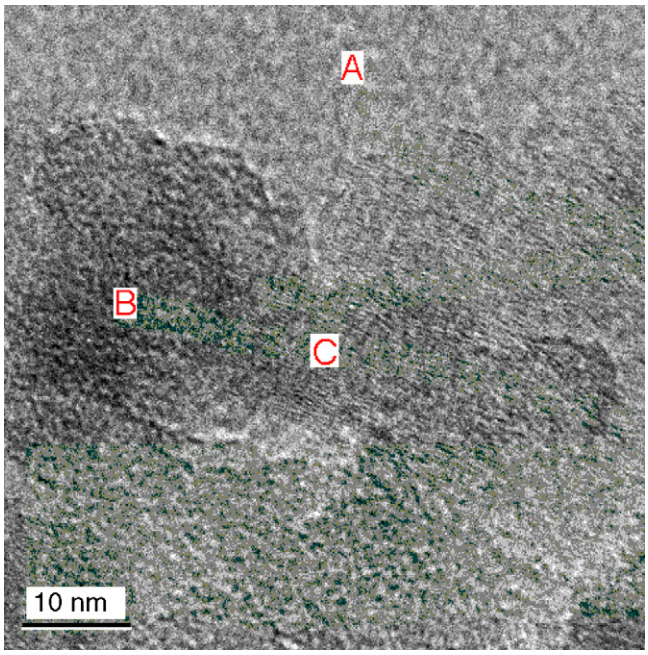

Fig. 9. HRTEM image of the soot heated to 700 °C.

3.3. Heat-induced changes in photo-deposited product

Heating of the photoproduct to 700 °C leads to a continuous weight loss starting from above 200 °C and a total weight decrease by 20%, which cannot be compatible with only H evolution, but indicate liberation of some carbonaceous structures [40]. The reorganization of soot structure and development of more sp^2 centers indicated by the Raman spectra is also supported by the Auger spectrum-derived proportion of the sp^2 C states that was found to increase from 33% to 60%. More apparent infrared spectral band at 1520 cm^{-1} (Fig. 8) reflects an increase of more conjugated structures [41,42]. These new features are consistent with transformation of amorphous phase into graphite as illustrated on HRTEM image of the soot (Fig. 9) showing three different regions A, B and C that we respectively ascribe to amorphous, concentric-like [12,15] and turbostratic structures. We note that the region C is indicative of graphene features.

Other IR spectral changes (Fig. 8)—the diminution of all bands with respect to absorption between 2850 and 3000 cm^{-1}, the change of the broad 1000–1250 cm^{-1} band to a narrow band peaked at 1060 cm^{-1} and a new weak band at 840 cm^{-1}, assignable to ν(Si–C) mode [39]—show substantial depletion of silica and C=O and C–O moieties and an increase of Si–C bonds in polyoxocarbosilane units. The additional heating of the carbon–silica–polyoxocarbosilane nanocomposite thus results in partial graphitization of carbon phase and a complete conversion of silica to polyoxocarbosilanes having more Si–C bonds than in the deposited carbon–silica–polyxocarbosilane soot.

3.4. Relation to similar classes of nanocomposites

The reported carbon–silica–polyoxocarbosilane and carbon–polyoxocarbosilane nanocomposites contain only low amounts of the Si/O components in amorphous or partly graphitized carbon and differ from the earlier reported silica-rich carbon–silica nanocomposites and diamond-like nanocomposite coatings. The former were prepared by carbonization inside silica pores [43], using sol–gel synthesis of silica–carbon precursor composites, followed by carbonization [44], by intercalation and hydrolysis of alkoxysilane in graphite oxide, followed by post carbonization [45,46] and by similar mechanochemical approach [47] and were recently designed as low cost solar absorbers [43,44] and novel class of catalytic systems [48]. The latter consist in networks of amorphous carbon and silica and were obtained as films from silicon–organic precursors in a plasmatron [49] and by ion-beam assisted deposition in ethyne [50] and they represent thermally stable systems [51], wherein the two networks stabilize each other by weak chemical forces.

We stress that nanosized carbon–polyoxocarbosilane composites have not been particularly examined so far, although their bulk counterparts are accessible by pyrolysis of siloxanes [52,53] or sol–gel organosilicon polymers [54,55] and are useful intermediates to silicon carbide.

4. Conclusions

The ArF laser-photolysis of 1,3-butadiyne leads to efficient chemical vapor deposition of nanosized amorphous carbon soot incorporating silica and polyoxocarbosilane ingredients.

The volatile “side-products”—polyynes, cumulenes and ethynylbenzene are considered intermediates to soot formation; GC/MS detection of 1,2,3-butatriene represents the first experimental evidence on the up to now elusive cumulenes.

The incorporation of silica and polyoxocarbosilane ingredients into nano-carbon soot occurs through silica etching by photolytic products, the process that has not been yet described for the gas phase.

Heating of the deposited photoproduct leads to development of more sp^2 carbon centers and ordering in cyclic structures, as well as a complete conversion of silica ingredient to polyooxocarbosilane.

The described procedure can initiate more interest in laser photolytic production of nanocomposites through etching of materials transparent to laser radiation by photolytic products.

Acknowledgements

This work was supported by GA ASCR Grant No. 400720619. The authors thank Dr. O. Šolcová for surface area measurements.

References

[1] K. Kitahama, K. Hirata, H. Nakamatsu, S. Kawai, N. Fujimoro, T. Imai, H. Yoshino, A. Doi, Appl. Phys. Lett. 49 (1986) 634–635.
[2] K. Kitahama, Appl. Phys. Lett. 53 (1988) 1812–1814.
[3] B. Dischler, E. Bayer, J. Appl. Phys. 68 (1990) 1237–1241.
[4] J. Pola, A. Ouchi, K. Saito, K. Ishikawa, Y. Koga, Chem. Phys. Lett. 262 (1996) 279–283.
[5] M. Lindstam, M. Boman, K. Piglmayer, Appl. Surf. Sci. 138/139 (1999) 413–417.

[6] M. Lindstam, M. Boman, K. Piglmayer, Thin Solid Films 394 (2001) 115–124.
[7] G. Stenberg, K. Piglmayer, M. Boman, J.-O. Carlsson, Appl. Surf. Sci. 109/110 (1997) 549–553.
[8] V. Dřínek, M. Urbanová, Z. Bastl, I. Gregora, V. Vorlíček, J. Šubrt, J. Pola, Appl. Phys. A 66 (1998) 503–509.
[9] P.R. Buerki, S. Leutwyler, Surf. Coat. Technol. 47 (1991) 22– 28.
[10] I. Morjan, I. Voicu, F. Dumitrache, I. Sandu, I. Soare, R. Alexandrescu, E. Vasile, I. Pasuk, R.M.D. Crydson, H. Daniels, B. Rand, Carbon 41 (2003) 2913–2921.
[11] A. Galvez, N. Herlin-Boime, C. Reynaud, C. Clinard, J.N. Rouzaud, Carbon 40 (2002) 2775–2789.
[12] N. Herlin, I. Bohn, C. Reynaud, M. Cauchetier, A. Galvez, J.N. Rouzaud, Astron. Astrophys. 330 (1998) 1127–1135.
[13] M. Choi, I.S. Altman, Y.J. Kim, P.V. Pikhitsa, S. Lee, G.S. Park, T. Jeong, J.-B. Yoo, Adv. Mater. 16 (2004) 1721–1725.
[14] M. Ehbrecht, M. Faerber, F. Rohmund, V.V. Smirnov, O. Stellmakh, F. Huisken, Chem. Phys. Lett. 214 (1993) 34–38.
[15] I. Morjan, I. Voicu, R. Alexandrescu, I. Pasuk, I. Sandu, F. Dumitrache, I. Soare, T.C. Fleaca, M. Ploscaru, V. Ciupina, H. Daniels, A. Westwood, B. Rand, Carbon 42 (2004) 1269–1273.
[16] K. Kwok, W.K.S. Chiu, Carbon 43 (2005) 437–446.
[17] F. Rohmund, R.E. Morjan, G. Ledoux, F. Huisken, J. Vac. Sci. Technol. B 20 (2002) 802–811.
[18] J.B. Armitage, E.R.H. Jones, M.C. Whiting, J. Chem. Soc. (1951) 44–48.
[19] J. Pola, A. Ouchi, Z. Bastl, K. Vacek, J. Boháček, H. Orita, Carbon 42 (2004) 2521–2526.
[20] J. Wang, H. Niino, A. Yabe, Appl. Phys. A 111 (1999) 111–113.
[21] H. Niino, Y. Kawaguchi, T. Sato, A. Narazaki, T. Gumpenberger, R. Kurosaki, Appl. Surf. Sci. 252 (2006) 4387–4391.
[22] R. Böhme, S. Pissadakis, D. Ruthe, K. Zimmer, Appl. Phys. A 85 (2006) 75–78.
[23] H.L. Woodcock, H.F. Schaefer III, P.R. Schreiner, J. Phys. Chem. 106 (2002) 11923–11931.
[24] S. Glicker, H. Okabe, J. Phys. Chem. 91 (1987) 437–440.
[25] R.F.C. Brown, Pyrolytic Methods in Organic Chemistry, Organic Chemistry Monographs, vol. 41, Academic Press, New York, 1980.
[26] F. Stahl, P.v.R. Schleyer, H.F. Schaefer III, R.I. Kaiser, Planet. Space Sci. 50 (2002) 685–692.
[27] G. Apavdin, W.H. Fink, W.M. Jackson, J. Chem. Phys. 121 (2004) 9368–9377.
[28] J. Schwan, S. Ulrich, K. Jung, H. Ehrhardt, R. Samlenski, R. Brenn, Diamond Relat. Mater. 4 (1995) 304–308.
[29] P.K. Bachmann, D.U. Wiechert, in: R.E. Clausing, al. et (Eds.), Diamond and Diamond-Like Films and Coatings, Pergamon Press, 1991, p. 677.
[30] A.C. Ferrari, J. Robertson, Phys. Rev. B 61 (2000) 14095–14107.
[31] J. Schwan, S. Ulrich, V. Batori, H. Ehrhardt, J. Appl. Phys. 80 (1996) 440–447, and refs therein.
[32] R.O. Dillon, J.A. Woollam, V. Katkanant, Phys. Rev. B 29 (1984) 3482–3489.
[33] E.L. Galeener, G. Lucovsky, Phys. Rev. Lett. 37 (1976) 1474–1478.
[34] C.D. Wagner, Practical surface analyses, in: D. Briggs, M.P. Seah (Eds.), Auger and X-ray Photoelectron Spectroscopy, vol. 1, Wiley, Chichester, 1994, p. 595.
[35] J. Pola, A. Galíková, A. Galík, V. Blechta, Z. Bastl, J. Šubrt, A. Ouchi, Chem. Mater. 14 (2002) 144–153.
[36] M.R. Alexander, R.D. Short, F.R. Jones, M. Stollenwerk, J. Zabold, W. Michaeli, J. Mater. Sci. 31 (1996) 1879–1885.
[37] J.C. Lascovich, R. Giorgi, S. Scaglione, Appl. Surf. Sci. 47 (1991) 17–21.
[38] B. Velde, R. Couty, J. Non-Cryst. Solids 94 (1987) 238–250.
[39] R.G.J. Miller, H.A. Willis (Eds.), Infrared Structural Correlation Tables and Data Cards, Heyden & Son Ltd., Spectrum House, London, 1969.
[40] X. Jiang, W. Beyer, K. Reichelt, J. Appl. Phys. 68 (1990) 1378–1380.
[41] M. Gussoni, C. Castiglioni, G. Zerbi, in: R.J.H. Clark, R.E. Hester (Eds.), Spectroscopy of Advanced Materials, Wiley, New York, 1991, p. 251.
[42] Z.L. Akkerman, H. Efstathiadis, F.W. Smith, J. Appl. Phys. 80 (1996) 3068–3075.
[43] Y. Mastai, S. Polarz, M. Antonietti, Adv. Funct. Mater. 12 (2002) 197–202.
[44] G. Katumba, J. Lu, L. Olumekor, G. Westin, E. Wackelgard, J. Sol–Gel Sci. Technol. 36 (2005) 33–43.
[45] Z.M. Wang, K. Hoshino, K. Shishibori, H. Kanoh, K. Ooi, Chem. Mater. 15 (2003) 2926–2935.
[46] Z.M. Wang, K. Shishibori, K. Hoshinoo, H. Kanoh, T. Hirotsu, Carbon 44 (2006) 2479–2488.
[47] Y.H. Chu, Z.M. Wang, M. Yamagushi, H. Kanoh, T. Hirotsu, Y.X. Zhang, Langmuir 21 (2005) 2545–2551.
[48] M.L. Anderson, R.M. Stroud, D.R. Rolison, Nano Lett. 2 (2002) 235–240.
[49] V.F. Dorfman, Thin Solid Films 212 (1992) 267–273.
[50] X.Z. Ding, F.M. Zhang, X.H. Liu, P.W. Wang, W.G. Durrer, W.Y. Cheung, S.P. Wong, I.H. Wilson, Thin Solid Films 346 (1999) 82–85.
[51] W.J. Yang, Y.H. Choa, T. Sekino, K.B. Shim, K. Niihara, K.H. Auh, Thin Solid Films 434 (2003) 49–54.
[52] F.I. Hurwitz, P. Heimann, S.C. Farmer, D.M. Hembreem, J. Mater. Sci. 28 (1993) 6622–6630.
[53] G.T. Burns, R.B. Taylor, Y. Xu, A. Zangvil, G.A. Zank, Chem. Mater. 4 (1992) 1313–1323.
[54] E. Breval, M. Hammond, C.G. Pantano, J. Am. Ceram. Soc. 77 (1994) 3012–3018.
[55] G.D. Soraru, G. D'Andrea, R. Campostrini, F. Babonneau, G. Mariotto, J. Am. Ceram. Soc. 78 (1995) 379–387.